WideScatter:Toward Wide Area Battery-Free Wireless Sensor Networks

Ali Saffari

A thesis
submitted in partial fulfillment of the
requirements for the degree of

Master of Science

University of Washington

2021

Committee:

Joshua R. Smith

Saman Naderiparizi

Program Authorized to Offer Degree:
Electrical Engineering

University of Washington

Abstract

WideScatter:Toward Wide Area Battery-Free Wireless Sensor Networks

Ali Saffari

Chair of the Supervisory Committee:

The vision of ubiquitous battery-free sensing has run into the practical limitations of wireless communication networks. To address this, we design the first wide-area and scalable backscatter network with multiple receivers(RX) and transmitters(TX) base units to communicate with battery-free sensor nodes. Our system circumvents the inherent limitations of backscatter systems - including the limited coverage area, frequency-dependent operability, and sensor node limitations in handling network tasks- by introducing several coordination techniques between the base units starting from a single RX-TX pair to networks with many RX and TX units.

We build low-cost RX and TX base units and battery-free sensor nodes with multiple sensing modalities and evaluate the performance of the WideScatter system in various deployments. Our evaluation shows that we can successfully communicate with battery-free sensor nodes across 23400 ft^2 of a two-floor educational complex using 5 RX and 20 TX units, costing $569. Also, we show that the aggregated throughput of the backscatter network increases linearly as the number of RX units and the network coverage grows.

TABLE OF CONTENTS

LIST OF FIGURES

ACKNOWLEDGMENTS

Mohamad Katanbaf and I worked on this project and submitted our results to the 19th ACM International Conference on Mobile Systems, Applications, and Services (MobiSys 2021). I would like to thank my advisor, Professor Joshua Smith, Saman Naderiparizi, my first mentor, Mohamad Katanbaf, Zerina Kapetanovic, Vikram Iyer, Mehrad Hessar, Ali Najafi, and other Sensor Systems Lab members.

Chapter 1

INTRODUCTION

Recent advances in energy harvesting, physical sensors, wireless networks, data processing, and machine intelligence picture a future where billions of everyday objects turn into smart, connected devices that can sense their surroundings, communicate their data, and react to human interactions and other environmental stimuli. This vision, however, has run into practical limitations of wireless communication networks.

An ideal wireless technology for a battery-free or self-powered [1] sensor network should possess two essential qualifications: the sensor nodes should consume very little energy since the harvested energy is scarce, and the infrastructure to communicate with the sensor nodes should be low-cost to make widespread adaptation feasible. Current commercial wireless technologies do not satisfy these two objectives simultaneously. Active radios, such as BLE, Zigbee, or LoRa compliant radios, consume too much energy and are not suitable for battery-free solutions, while passive RFID systems are expensive and result in high infrastructure cost to cover a practical setting [9].

Recent bistatic backscatter systems [23, 30, 33, 77, 56] have shown promise to find a middle-ground to this challenge by employing the backscatter technology to reduce the energy burden of wireless communication, while leveraging the economies of scales and ubiquity of industry-standard protocols such as WiFi, Bluetooth, ZigBee, and LoRa to reduce the cost of reader infrastructure. Bistatic backscatter systems still suffer from a shorter communication range than conventional active radios, and a single receiver (RX)-transmitter (TX) pair is insufficient to cover a multi-bedroom or multi-floor house. The limited coverage of bistatic

[1] A system that harvests enough energy for its operation, but might use a rechargeable battery to store the energy.

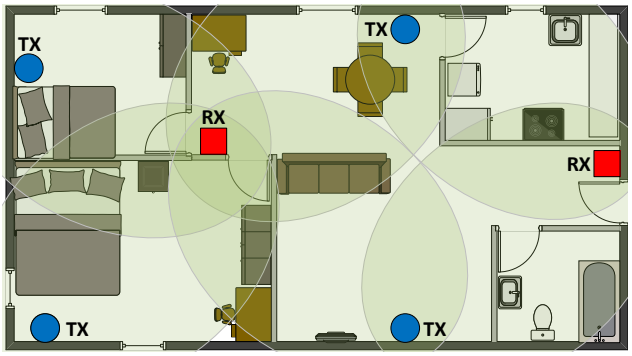

Figure 1.1: **We deploy several RX (red squares) and TX (blue circles) base units to extend the coverage of low-cost bistatic backscatter networks and deliver seamless connectivity to battery-free sensor nodes.**

backscatter systems complicates the user experience and limits the use cases for backscatter systems.

In this work, we present WideScatter, the first scalable bistatic backscatter network for battery-free sensing, where a network of low-cost RX and TX base units is employed to deliver backscatter connectivity to many battery-free sensor nodes over a wide area. This seamless coverage addresses one of the remaining challenges in using backscatter systems and creates many new opportunities in smart homes and smart buildings by enabling peripheral, wearable, and medical devices such as pill bottles [51] and insulin pens [17, 38] to use backscatter to transfer their data to the cloud. To the best of our knowledge, this is the first work that discusses and implements a bistatic backscatter network with multiple RX and TX base units.

Using multiple base units to cover a larger area has been implemented in cellular [57, 5] and WiFi [55, 10] networks for a long time. To understand the difference between these solutions and our backscatter solution, we need to take a closer look at how the bistatic backscatter works. In a backscatter deployment, a transmitter generates the carrier, a sensor node synthesizes packets by reflecting the carrier, and a receiver demodulates the backscattered packets. Thus, the base units could be divided into two groups in bistatic backscatter

systems, TX units, and RX units. Coordination between TX and RX units is necessary to implement features such as frequency hopping, time-division multiplexing, etc. Furthermore, the wireless signal propagates twice in a backscatter system, from TX to sensor node and from the sensor node to RX, resulting in a significantly higher propagation loss and reduced communication range than active radios. Also, the TX carrier signal appears as a strong interference to the RX. The high propagation loss and strong interference further complicate the bistatic backscatter deployments, especially in rich multipath indoor environments. Finally, the sensor nodes in backscatter systems have strict energy limitations, while the base units have higher computational and energy resources. This imbalance requires the system to push the network management tasks to the base units while keeping the sensor nodes as simple as possible.

We notice that unlike a cellular base station that covers a circle around itself, the coverage area of the backscatter system is almost entirely limited to the area between the TX and RX units (see Fig. 2.1). This difference means that we do not need another TX-RX pair to double the coverage area of a bistatic backscatter system. We only need to add a second TX unit and share one RX unit between the two TX units (or vice versa). We extend this idea of sharing TX units and RX units among one another, to form a network of many TX and RX units that covers more extensive areas, as shown in Fig. 1.1. This solution still uses backscatter to communicate with the sensor nodes, which reduces the energy harvesting barrier for a practical solution. Although this solution needs multiple base units similar to an RFID solution, each TX or RX base unit is significantly cheaper than an RFID reader.

In this work, we equip the RX units with more processing and communication capabilities and rely on them to manage the operation of TX units and sensor nodes. RX units receive the sensor data and have direct access to the data and channel information, which gives them a clear advantage over the TX units for managing the network. In the simple case of one RX and one TX unit, we use the RX unit to select the frequency and carrier power for each backscatter attempt to maximize communication reliability with the sensor nodes and overcome frequency-selective fading. RX units also manage the time to communicate

with multiple sensor nodes through time-division multiplexing. In the case of one RX and several TX units, the RX also needs to track which TX-sensor node combinations result in a successful communication to select the best TX unit for communicating with each sensor node. Finally, in the multiple RX and multiple TX case, the RX units coordinate with each other to assign sensor nodes amongst themselves, and keep track of the movements and variations in the network. We implement RX units, TX units, and sensor nodes that support these functionalities to achieve large-scale backscatter coverage.

Our primary motivation in using backscatter is to relax energy harvesting requirements on the sensor nodes. Previous works have shown the possibility of battery-free solutions by combining backscatter with low-power sensors such as microphones [71] and cameras [65, 22]. However, these works use analog modulations tailored for the specific sensor data. This work presents a sensor node platform that communicates with our base units through 802.15.4g packets and can accommodate many different sensors, including cameras, microphones, and environmental sensors such as temperature, humidity, and illuminance sensors. Our sensor nodes are equipped with an ultra low power radio to wake them from sleep mode, which allows them to operate entirely on the energy harvested from a $2in^2$ solar cell under indoor light intensity levels.

Previous long-range backscatter deployments have been proposed in [70, 73, 56, 23]. These implementations use a single TX-RX pair and extend the communication range by lowering the receiver sensitivity. However, this is not a desirable solution since it reduces the communication data rate and throughput of the system. In this work, we extend the backscatter deployment coverage while maintaining the high data rate for sensor nodes.

We implement the WideScatter system using COTS components and deploy it in several indoor environments. Our evaluation shows that the sensor node consumes 9 uA in the listening mode and 802 uA in backscatter mode while communicating with RX and TX base units 150 ft away. Results are summarized below:

• WideScatter covers an $800ft^2$ single bedroom apartment with 125 Kbps backscatter links using 1 RX unit and 4 TX units, for a total cost of $114 at low volumes. It can cover a

$23400 ft^2$ educational complex using 5 RX units and 20 TX units for a total cost of $569.

• The modular battery-free sensor node accommodates multiple sensors, including image and audio sensors. It can send the temperature, humidity, and illuminance data every second using the energy harvested from a 2 in^2 solar cell.

• We show that the aggregated throughput of the backscatter network increases by using more RX units. Using 5 RX units, our backscatter network collects data from multiple sensors at an aggregated rate of up to 375 Kbps, 4.17 times faster than a single sensor node throughput.

Chapter 2

BACKSCATTER PRIMER

Backscatter sensor nodes rely on reflecting external RF signals for data transmission instead of generating a local RF signal. This reduces the power consumption and cost of wireless communication significantly and enables battery-free sensing systems [33, 30, 70]. Unlike conventional wireless networks where the communication happens between two devices- an access point and a mobile device- three devices are involved in a backscatter communication; a TX unit that generates the carrier signal, a backscatter sensor node that modulates and reflects the carrier, and an RX unit that listens to, and decodes the sensor node data.

One of the main challenges in backscatter systems is the strong interference at the receiver due to the carrier signal. Bistatic, or half-duplex, backscatter systems rely on physical separation of the TX and RX units to reduce the carrier interference [33, 30, 70], while monostatic, or full-duplex, backscatter systems rely on self-interference cancellation circuits for this purpose [32, 8, 12]. Another popular technique to mitigate the carrier interference is using sub-carrier modulation at the sensor node [33, 30, 70, 32, 12, 77, 73, 24] to generate the backscatter packet at a frequency offset from the carrier signal. This technique pushes the carrier signal out of the desired band at the receiver and reduces the receiver's sensitivity loss, since receivers can tolerate out-of-band interference.

The coverage of a bistatic backscatter system depends on the relative distance of the RX and TX units[33, 31]. We use the free-space signal propagation model to plot the backscatter coverage in four different cases in Fig. 2.1. The RX and TX locations are shown with circles of the same color in each case. When the TX and RX are too close to each other, they completely cover the area between themselves, but the carrier interference limits

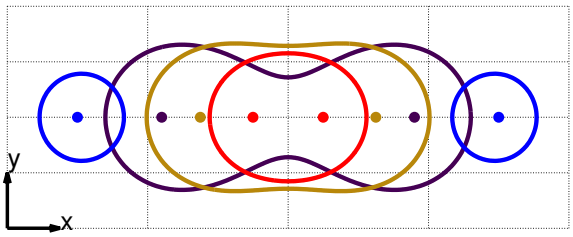

Figure 2.1: **Backscatter coverage dependance on the RX-TX distance. Placing the RX-TX too close (red) or too far (purple and blue) results in non-optimal coverage scenarios.**

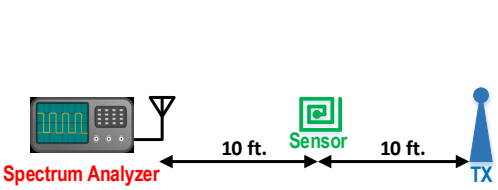

(a) Experiment setup

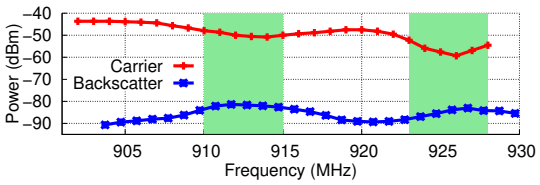

(b) Carrier and backscatter signal power at the RX.

Figure 2.2: **The effect of multi-path fading on backscatter link. Frequency bands with lower carrier power and higher backscatter power are most suitable for backscatter communication.**

the coverage area (red plot). As the RX-TX distance increases, the coverage area expands to reach its maximum (brown plot). If we further increase the RX-TX distance, first the coverage width at the center starts to shrink (purple plot), and finally, we lose the coverage at the center and the coverage map becomes disjoint (blue plot). Although we use the free-space propagation model for this analysis, it highlights the importance of RX and TX units placement in covering large spaces with backscatter connectivity.

The wireless propagation in indoor environments is subject to multipath fading. To show the effect of the multipath fading, we perform a simple experiment. We set a transmitter to generate a CW carrier signal, and a backscatter node, placed 10 ft away from the TX,

to reflect the TX signal at 1.7 MHz offset frequency, as shown in Fig. 2.2(a). We use a spectrum analyzer, placed 10 ft away from the backscatter node, to measure the carrier and corresponding backscatter signal powers. Fig. 2.2(b) shows the carrier and backscatter signal power as we sweep the carrier frequency from 902 MHz to 928 MHz. The backscatter (i.e., desired) signal power varies 10dB in this experiment, while the carrier (i.e., interference) signal power varies 15dB. The two signal powers are independent of each other, and their peaks and valleys happen at different frequencies. The best frequency bands for backscatter communication are the ones with maximum backscatter signal power and minimum carrier signal power. If the RX blocker tolerance at 1.7 MHz frequency offset is 35 dB, we can see that only some of the frequency channels are operative for backscatter links, as shown with green strips in Fig. 2.2, which could be enough for most narrow-band, low data rate applications. This experiment shows the importance of selecting communication parameters, such as frequency, to minimize communication error rates for low-power sensor networks [14].

Chapter 3
SYSTEM DESIGN

This section describes the backscatter network architecture used to cover a wide area and communicate with many sensor nodes. We start with one RX-TX pair and extend the coverage first by adding more TX units and finally by including more RX units. Throughout this section, we assume that each sensor node has a unique identification number (ID), and the backscatter network has prior knowledge of the sensor nodes' IDs.

3.1 Single RX - Single TX

In the simplest form, a bistatic backscatter system consists of one RX unit, one TX unit, and one or several sensor nodes. The RX and TX should coordinate with one another to achieve three main functionalities: improving the link reliability, time-frequency alignment, and handling retransmissions. We use a wireless back-channel between the RX and TX units to communicate and coordinate between the two devices.

The communication cycle of the system is shown in Fig. 3.1. It starts with selecting the optimum parameters for the frequency channel and carrier power to maximize link throughput and minimize the error rate in communicating with the specified sensor node. The RX uses scores calculated based on the results of previous communication cycles for this purpose. The RX selects the frequency channel with the highest score that satisfies the frequency hopping requirements of the regulatory mandates. It also finds the carrier power with the highest success rate and uses it as the center of probability distribution to select the carrier power (Fig. 3.1(a)). After selecting the communication parameters, the RX shares them with the TX unit. The TX unit has been in listening mode until it receives an activation packet from the RX unit on the back-channel. The activation packet also specifies the duration of

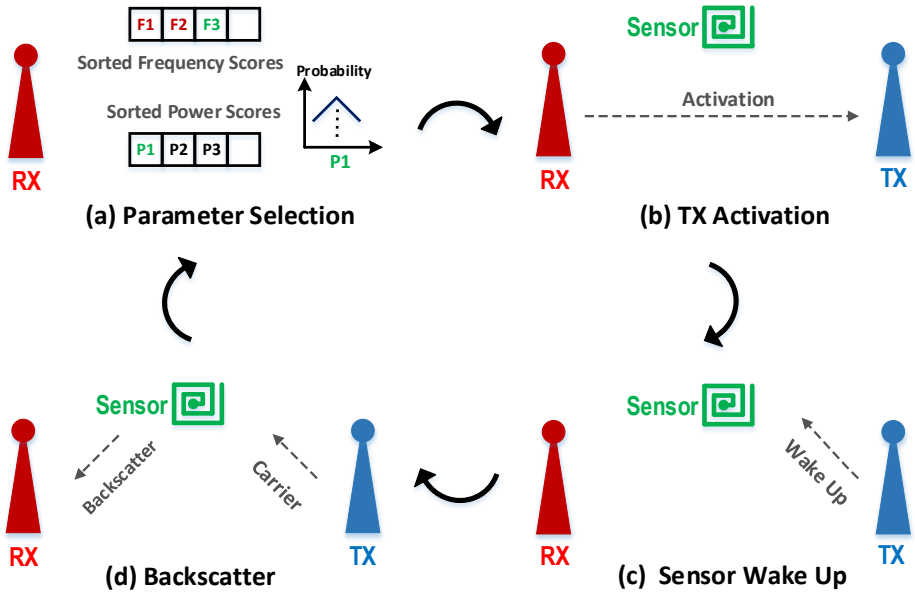

Figure 3.1: **Backscatter Communication cycle.**

the carrier signal that the TX unit has to generate, as well as the sensor node identification number and the command for the sensor node (Fig. 3.1(b)). Once the TX unit receives the activation packet, it sends a packet to the sensor node, which contains the sensor node ID and the requested command, to wake the sensor node (Fig. 3.1(c)). Finally, the sensor node wakes up, receives the command, and responds appropriately by transmitting one or several backscatter packets. During this period, the TX generates the carrier signal, and the RX listens for the backscatter packets (Fig. 3.1(d)). When the backscatter duration is over, the RX unit analyzes the received packets based on the command issued to the sensor node and decides whether retransmission is required or not. It also updates the frequency and power score vectors based on the communication cycle results. The devices follow the same cycle for the subsequent communications between them.

The first step of the communication cycle is to select backscatter frequency and power level. This step is vital to improve the overall throughput and reliability of the system since

backscatter and carrier signal strengths at the receiver vary significantly at different frequency channels due to the multipath in indoor environments, as mentioned in sec. 2. Similarly, the carrier power could affect the performance of the backscatter communication too. Increasing carrier power increases both the backscatter signal power and TX carrier interference at the RX unit at the same time, and might improve or deteriorate the performance of the backscatter link [31]. We assign a success score to each communication cycle based on the ratio of the successfully received packets to the total expected packets, and update the score for the frequency channel and power level used in the cycle with a moving average formula. To explore the entire space of possible frequency and power values, we set an exploration probability based on the error rate over a predefined number of previous communication cycles. In exploration mode, we select the two parameters randomly [30].

The communication cycle allows the RX unit to control the TX carrier frequency, start time and duration through the activation packet. This control is essential for two reasons. First, the TX unit can not generate the carrier signal indefinitely since it would waste energy and generate too much interference for other wireless users in the vicinity. The TX unit should only generate the carrier when required by the sensor node, which means the devices should be time-aligned to utilize the spectrum and energy resources efficiently. Furthermore, the TX has to hop between different frequencies in the ISM band to satisfy regulatory mandates. Since the desired signal frequency at the RX is equal to the TX frequency plus the subcarrier modulation frequency of the sensor node [33, 30, 70], the RX needs to know these two values in order to frequency align itself with the other devices. Using the activation packet to initiate and control the TX operation guarantees time and frequency alignment between the devices.

In the proposed communication cycle, the RX unit sends the sensor node command to the TX unit, and the TX unit passes the command to the sensor node. Thus, the data communication effectively happens between the RX unit and the sensor node, with the TX unit facilitating the data transfer between them. The two base units have different capabilities in a bistatic backscatter network. The RX unit demodulates the backscatter

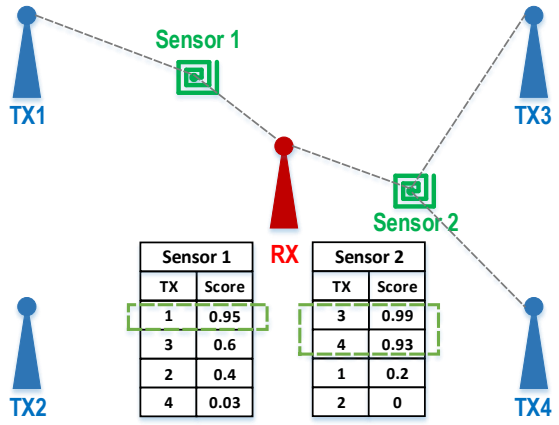

Figure 3.2: **Selecting a TX unit in a single RX - multiple TX scenario. We select the TX unit based on the assigned confidence score to each TX unit - sensor node combination.**

signal and detects whether the desired packet is successfully received or failed, and the TX unit can communicate with the sensor node. By using the TX unit as a relay, the RX unit has complete control to ask for retransmissions.

3.2 Single RX - Multiple TX

The system described in sec. 3.1 highlights the fact that the data exchange happens between the RX unit and the sensor nodes. Thus, adding more TX units to the system improves the backscatter system coverage without significantly affecting the system architecture. The RX unit still controls the operation of the system, and it must select one more parameter, the TX unit, at the start of each communication cycle.

To compare the performance of different TX nodes in communicating with each sensor node, we assign a confidence score to each TX unit. The confidence scores are initialized to 1 and updated with an exponential moving average formula using the cycle success rate each time the TX unit-sensor node combination is used. Fig. 3.2 shows sample confidence tables

in the single RX - multiple TX arrangement for two sensor nodes. The RX unit uses the frequency and power score vectors to prioritize and select channels with superior performance in communicating with the backscatter sensor nodes. The scores depend on the geometrical placement of the devices with respect to each other and change based on the selection of the TX unit. Thus, it needs to record one set of these score vectors for each TX unit-sensor node combination.

We follow the following procedure to select a TX unit based on the confidence table at the start of the communication cycle. First, we select the TX units with confidence scores higher than 0.9. If the set has more than one member, we use a weighted random selection to select one of them. If the set has no member, we filter out the TX units with confidence scores less than 0.2 times of the maximum confidence score, and use a weighted random selection to select one of the remaining TX units. Once the TX unit is selected, we follow the communication cycle, as explained in sec. 3.1, with the selected TX unit. We assign a unique ID to each TX unit and include the transmitter ID in the activation packet.

Similar to the single RX-single TX architecture, the TX units are in listening mode until they receive the activation packet. The TX units only move forward with transmitting the carrier if their ID is matched to the one in the activation packet. Otherwise, they discard the activation packet and return to the listening mode.

3.3 Multiple RX - Multiple TX

Increasing the number of TX units around one RX unit allows us to expand the backscatter coverage around the RX unit in different directions. However, we can only achieve a truly scalable system and cover areas beyond the reach of a single RX-TX pair by employing more than one RX unit. In the Multiple RX - Multiple TX arrangement, we break the area that we need to cover into several sections and use one RX unit with one or multiple TX units to cover each section.

Similar to cellular networks, a sensor node might move between these sections. Since the backscatter sensor nodes do not have the hardware or energy resources to determine the

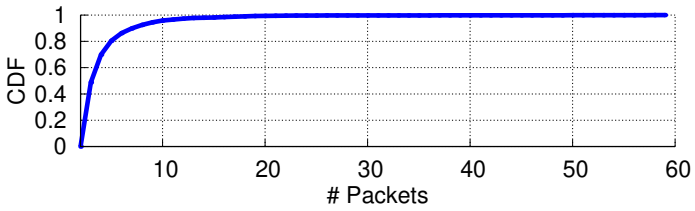

Figure 3.3: **Distribution of number of consecutive dropped packets when the sensor node moves within one section.**

link quality metrics, the base units have to handle the handover. We add a central unit, or server, that assigns the sensor nodes to the RX units and updates these assignments as the sensor nodes move. We equip the RX units with WiFi and use it as the backhaul link to communicate with the server.

Once a sensor node moves from section A to section B, we need to change its assigned RX unit. For this purpose, first, the RX_A must detect that the sensor node is missing, and then, the RX_B must search for the sensor node and successfully communicate with it. A sensor node could move to any other section between two communication cycles in a backscatter network, since the sections are small and the time interval between communication attempts could be long.

We use the number of consecutively dropped packets as the metric to detect a sensor node is disconnected from its assigned RX unit since once a sensor node leaves a given section, all backscatter communication attempts with that sensor would fail. There is a trade-off in selecting the threshold to announce the disconnection to the server. Higher thresholds waste network resources by trying to communicate with a sensor node that has left the section. On the other hand, lower thresholds result in false disconnection alarms, which have a high penalty because they result in unnecessary search events in other sections of the backscatter network. Also, moving the sensor within the boundaries of a section could result in multiple consecutive dropped packets since the base units have to find a different subset of operatable frequencies for the new location as described in sec.3.1. This further complicates the threshold selection.

To find the number of consecutive packets that could drop when the sensor node moves inside a section, we perform an experiment by moving the sensor node within the boundaries of one section 100 times in 5 different environments. Fig. 3.3 shows the distribution of more than three consecutive dropped packets during these movements. Based on this plot, sensor node movements within a section cause less than 20 consecutive dropped packets with a probability of 99.5%. Therefore, we set the threshold for detecting a missed sensor node at 20 consecutive dropped packets, which results in a false alarm rate of less than 0.5%.

An ideal search procedure should be fast and accurate. Due to the lack of existing knowledge about channel properties, the RX units have to try different frequency channels to increase the likelihood of successful communication with the sensor node at the new location. However, increasing the number of frequency channels in the search procedure would increase the search duration. Previous studies [41, 35] show that the multipath fading loss in indoor environments becomes uncorrelated as the frequency separation increases. To find the optimum number of frequency bands for the search procedure, we set up TX-RX base units at 12 different locations with 20 sensor node testing points (240 total) around them. For each setup, we set the carrier power at the maximum and try all the frequency bands between 902 MHz and 928 MHz with 400 KHz channel spacing to communicate with the sensor node at each point.

Fig 3.4(a) shows the distribution of number of operative bands over the 240 points, with 35% of the points not responding on any frequency and 13% of the points responding on all of them. We consider the points which respond on at least 10% of the frequency bands (150 points) as the target group and plot the probability of communicating with the sensor at these target points based on the number of attempted frequency channels in Fig 3.4(b). The figure shows that trying 9 channels results in 99% search accuracy. We consider some margin for errors in these experimental results and use 12 equally spaced frequencies in our search routine.

The server tracks the assigned RX unit for each sensor node. Once one of the RX units detects a missing sensor, it notifies the server. The server then randomly notifies one of the

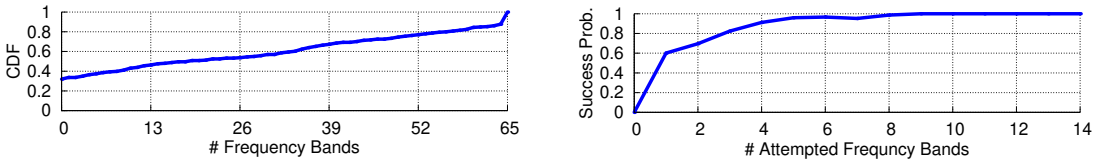

(a) Distribution of number of operative bands at 240 different tested locations.

(b) Probability of communication with a sensor node based on number of equal-distant frequency bands attempted.

Figure 3.4: **Selecting the number of frequency bands for the search procedure.**

other RX units to search for the missing sensor node and waits for the search result. If the search fails, the server notifies another RX unit, and this procedure continues until one of the RX units successfully communicates with the sensor node. The server holds a predefined period before notifying the same RX unit twice.

3.4 Base Units Placement

The primary target of the WideScatter system is residential and commercial buildings, where the area is most often divided into several sections with walls, partitions, or other obstacles. The RF signals attenuate as they pass through different materials. It is essential to consider the effect of these obstacles in the placement of the RX and TX units to achieve optimal performance. Here we suggest a few simple guidelines to place the base units and sensor nodes in the building.

- The RX and TX units should be far from each other to maximize the coverage area between them, but not too far to result in blind spots, as shown in Fig. 2.1. Backscatter coverage equations in [31] and propagation and attenuation measurements in [63, 7, 6] can be used for an initial starting point.
- It is best to keep the base units out of each other line-of-sight, as that would increase the carrier interference at the RX. The best performance is achieved if the sensor node is in

line-of-sight with both base units.

- The multipath in indoor environments helps the backscatter systems by creating a frequency-dependent non-flat attenuation profile, resulting in enough operative frequency bands for backscatter communication. Placing the base unit closer to walls or other large objects could improve backscatter performance.

Chapter 4

SENSOR NODE DESIGN

Our goal is to design a battery-free sensor node platform that can accommodate different sensors and communicate with the base units. We reduce the wireless power consumption of the sensor node by using low-power backscatter for the sensor node uplink and an ultra-low-power wake-up radio for the sensor node downlink. The wake-up radio allows the sensor node to stay in idle mode until the base units activate it. We also implement the gating technique to reduce the energy burden of power-hungry sensors by adding low-power auxiliary sensors. For example, a motion sensor is used to gate the operation of the camera. Finally, we use a low-power microcontroller with several communication protocols in our sensor node platform, which can easily interface with various commercial sensors.

FSK Backscatter. The sensor node transmits the data to the receiver using Frequency-Shift Keying (FSK) backscatter communication. In FSK backscatter, bits '0' and '1' are transmitted by changing the state of the RF switch connected to the antenna at frequencies f_0 and f_1. This results in a backscatter packet with $(f_0 + f_1)/2$ subcarrier modulation and $|f_0 - f_1|/2$ frequency deviation.

We use a temperature-compensated VCO to generate the variable frequency signal that controls the RF switch. A resistor sets the oscillator frequency, and we use two NMOS switches to control this resistance, as shown in Fig. 4.1. Switch Q1 controls the backscatter subcarrier modulation frequency, and switch Q2 sets the transmitted bit to '1' or '0'. We use the micro-controller SPI interface derived by the MCU crystal oscillator to generate accurate bit periods. Compare to using two individual oscillators to generate f_0 and f_1 frequencies [73], using a single controlled oscillator to generate both frequencies reduces the power consumption and ensures phase continuity in switching between the two frequencies.

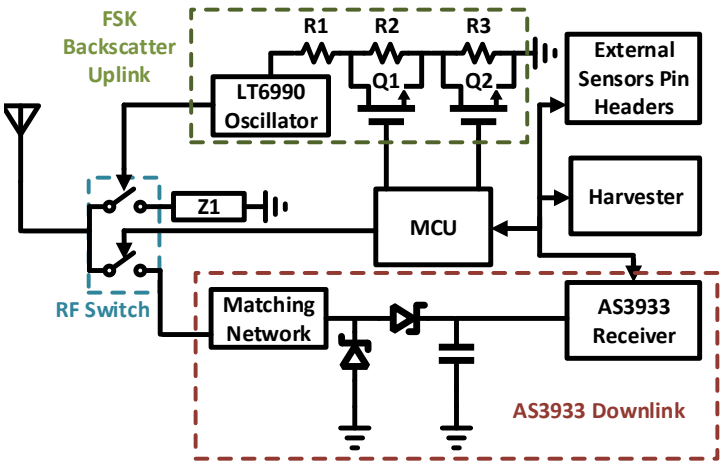

Figure 4.1: **Sensor node block diagram.**

Low Idle Power Consumption. The sensor node operates in the idle mode until it is activated by the base units to enable one of its sensors or report its latest recorded data. Therefore, our sensor nodes must be power efficient in the idle mode. Although the FPGAs allow us to implement custom communication protocols, they consume more power in the idle mode than the MCUs. We use a low-power MCU with several low-power idle modes in this work.

To wake up the MCU from the idle mode, we use a low-power and low-frequency wake-up radio [30]. While the MCU is in the idle mode, the wake-up radio listens to the packets transmitted by the TX units. If the received packet matches the sensor node's 16-bit ID, the radio generates an interrupt to the sensor node MCU and passes the received command to it.

Sensor Gating. We use low-power auxiliary sensors to gate the operation of the power-hungry sensors. For instance, a motion sensor can enable the operation of an image sensor when there is movement in the room. This helps us reduce the power consumption of the sensor node by limiting the operation of the power-hungry sensor (image sensor) to informative events. Similarly, the microphone activates only when the sound intensity passes a defined threshold.

We also implement second gating criteria by monitoring the energy storage element of the sensor node. The MCU measures the voltage of the energy storage element and sends it back to the base units in response to each sensor enable command. The base units monitor this voltage and use it to gate the commands issued to the sensor node. If the voltage falls below a defined threshold, the base units bypass the sensor readings requests from that sensor node and allow the energy harvesting unit to charge the storage element. The base units continue to monitor the energy storage voltage with a more extended reading period and resume regular operation once the voltage reaches a certain level.

Energy Harvesting. The energy harvesting unit of the sensor node collects energy from ambient light and stores it on an energy storage element. The energy storage element connected to each sensor node should store enough energy to support reading the physical sensors connected to the sensor node and transmitting their data to the base units. While supercapacitors have longer life cycles and can be employed to build truly battery-free sensor nodes, rechargeable batteries have higher energy capacity and can tolerate longer energy drought periods [78, 58]. Our energy harvesting unit can work with both types of energy storage elements.

Modular Design. We follow a modular design approach to building our sensor nodes. The MCU, wireless communication units, temperature, humidity, and illuminance sensors are placed together as the basic sensor node. The energy harvesting unit, camera, and microphone sensors are designed as add-on boards that mount on top of the basic sensor node through 5 power and 12 Input/Output (IO) pins (see Fig. 5.1(c)-(e)). The modular design allows us to support more sensors without redesigning the communication section.

Regulatory requirements limit the channel dwell time to 400 ms at each frequency hop. However, sensors such as image sensor might require more time to transmit their entire data. Our firmware implementation breaks down the sensor data into multiple packets- the total number of the packets depends on the length of data- and transmits them to the receiver using backscatter communication. Also, in cases where one sensor node is equipped with

multiple sensors, the base units can separately request each sensor information.

Chapter 5
IMPLEMENTATION

We implement the WideScatter, consisting of the RX base units, TX base units, and sensor nodes, for operation in 902-928 MHz ISM band on 4-layer FR4 PCB. The system uses FSK modulation and 802.15.4g packet structure with seven preamble bytes, 16 CRC bits, and no whitening for communication between devices.

5.1 Base Units

Receiver Units. The RX unit has two parts, a communication board with the CC1352R wireless MCU, and a Raspberry Pi 4B single-board computer (RPi) with 2GB RAM for processing and backhaul. The two boards are connected to each other, as shown in Fig. 5.1(a), and communicate through a 1Mbps serial link. The CC1352R is a flexible receiver that supports FSK modulation with data rates from 0.3 to 1985 Kbps and RX filter bandwidths from 4.3 to 3767 KHz. The RX filter bandwidth determines the carrier attenuation and should be set accurately considering the data rate, frequency deviation, and subcarrier modulation frequency. The RPi board runs the Raspbian operating system. It processes the received data from the sensor nodes and determines the activation packet parameters. The RPi sends out this information to the CC1352R MCU to start the communication cycle, and the CC1352R MCU passes the received backscatter packets to the RPi as they are received. We implement the data handling and communication control protocols explained in sec. 3 using Python 3.7, which runs on the RPi.

Transmitter Units. Each TX unit consists of a CC1312R sub-GHz wireless MCU that receives the activation packet and generates the carrier signal, and a SKY65313-21 power amplifier (PA) that amplifies the carrier signal up to 28 dBm. The board ground planes

distribute the heat generated by the PA and limit the PA surface temperature to $65°C$ in continuous operation at maximum output power in room temperature. Fig. 5.1(b) shows the fabricated TX unit.

Server. One of the RX units also handles the server tasks. We use the python socket.io protocol to handle the communication between the RX units and server.

Data Collection Scheduling. The data collection process from each sensor initiates when the sensor node marks the availability of new data or when a pre-defined timeout is reached. The data collection might take one or several iterations. At each iteration, the RX unit first checks all the ongoing data collection processes for completion. If a portion of the data is missing, the RX unit generates the commands to read the missing parts and stores them in a queue. Next, all the commands in the queue are executed, and the responses to each command are processed. Once the queue is empty, the iteration is completed. We use time-division multiple access to accommodate multiple sensor nodes. Each sensor node has a unique ID, and only one sensor node responds to the command from the RX unit at each cycle.

Cost Analysis. We design the WideScatter intending to reduce the infrastructure cost of a wide area backscatter network. Our analysis using pricing data from Octopart shows that at low volumes of 1,000 units, the TX and RX base units costs $16.1 and $49.6 (including $35 for the RPi), respectively. The number of base units required to cover a specific building depends on its floor plan. We provide two sample cases in sec. 6.

5.2 Sensor Node

We select STM32L071C8, an ultra-low-power ARM Cortex-M0+ MCU with 20 KBytes RAM, as the sensor node MCU. The memory capacity is enough to store one image frame or one second of audio recording. A 4 MHz external crystal generates the MCU clock. We use AS3933 wake-up radio for downlink, and LT6990 VCO for generating the backscatter uplink signal. The sensor node is also equipped with HDC2080 humidity and temperature sensor,

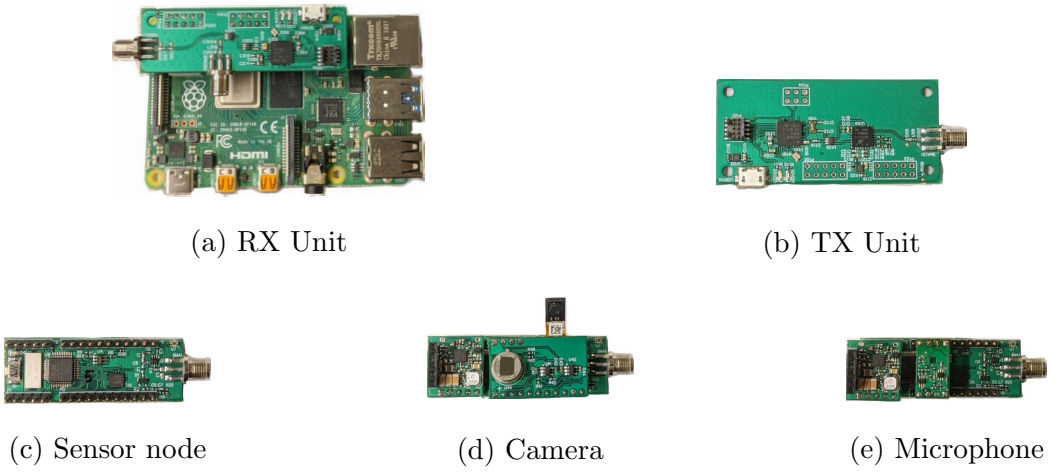

(a) RX Unit (b) TX Unit

(c) Sensor node (d) Camera (e) Microphone

Figure 5.1: **Prototype hardware.**

and opt3002 ambient light sensor. The sensor node is powered up using a 2.5 V regulator. We set the MCU core voltage to 1.2 V to reduce its power consumption. The antenna is shared between the wake-up-receiver downlink and backscatter uplink via the AS213-92LF RF switch, as shown in Fig. 4.1. A 47pF capacitor is chosen for $Z1$, which has a small impedance at the carrier frequency.

The sensor node supports four uplink data rates, 31.25 Kbps, 62.5 Kbps, 125 Kbps, and 250 Kbps. We use 1 MHz subcarrier modulation with 25 KHz frequency deviation for the two lower data rates, and 1.79 MHz subcarrier modulation with 80 KHz frequency deviation for the two higher data rates, by setting the values of R1, R2 and R3 to 26.7 $K\Omega$, 22.1 $K\Omega$ and 2.5 $K\Omega$, respectively.

In each communication cycle, the sensor node receives a one-byte command from the base units. Some commands invoke an action, such as taking a picture, while others request specific information, such as a portion of the recorded image. The sensor node includes the received command in its response to the base units for verification.

Energy Harvester. We design the energy harvesting unit with the BQ25570. We use a 100 mF super-capacitor and a 12 mAh Li-ion rechargeable battery as the energy storage

elements.

Camera. We use a Himax HM01B0 image sensor running in 160×120 *pixel* QQVGA mode as the main sensor, and a Panasonic EKMB1104111 motion sensor as the auxiliary gating sensor. Once the motion sensor is activated, or a take-picture command from the base unit is received, the MCU turns on the image sensor and enables its internal Phase-Locked Loop (PLL) to generate a 3 MHz clock for the image sensor. Once an image is captured, we turn off the motion sensor to avoid image overwrite and inform the base unit that an image is available. For data transmission, we divide one image into 12 large sections or 120 small sections, and the base unit can request a large or small section with a dedicated command as needed to complete reading the image. Once the base unit successfully receives the image, it re-activates the motion sensor.

Microphone. Our microphone board is designed with a VM1010 microphone sensor. The microphone has two operational modes, wake-up sound mode, and normal mode. In wake-up sound mode, which we use to gate the normal mode, it waits for an acoustic event to trigger the normal mode. The microphone records data for 1 second at 8 KS/s in normal mode. The transition between gating and normal modes and data transmission to the base unit are similar to the camera.

Chapter 6

EVALUATION

We perform several experiments to demonstrate the performance of the WideScatter system. First, we measure the power consumption of the sensor node with the camera module and evaluate the maximum sensor update rates using two solar cells with different sizes. Next, we evaluate the communication range of our system in line-of-sight and demonstrate the scalability of our solution in covering a two-floor educational complex. Also, we examine how deploying multiple RX and TX units affects the achievable aggregate throughput of the system. Finally, we show the handover performance when sensor nodes move in the network. We use omnidirectional whip antennas for all devices in our evaluations.

6.1 Power Consumption

We evaluate the sensor node power consumption using the camera module since it is the most power-hungry sensor. Our setup consists of one RX-TX pair and a sensor node. Fig. 6.1(a) shows the measured power that the camera consumes while capturing and transmitting one picture.

The operation of the camera starts in deep sleep mode, where it consumes 36 μW on average. At time = 0.06 second, the sensor node is activated to take a picture and transfer it to the MCU. This process takes 1.2 second, and the average power is 5.04 mW. PLL operation at the start and end of the process causes peaks in the power plot. Next, the RX unit requests transmission of the first section of the image, indicated with the blue rectangle in Fig. 6.1(a), at time = 2.1 second. This is followed by requests for transmission of the other 11 sections to complete the picture. The image transmission takes 1.69 second, and the average power during this time is 2.26 mW.

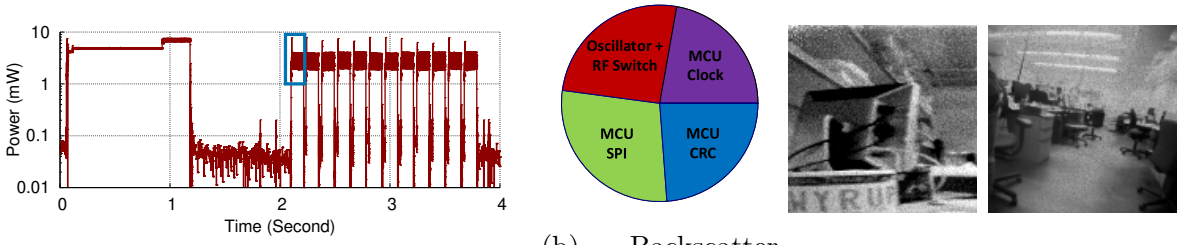

(a) Camera power consumption during one image

(b) Backscatter packet energy breakdown

(c) Sample images

Figure 6.1: **Battery-free camera evaluation results.**

Fig. 6.1(b) breaks down the energy that the sensor node consumes in transmitting a 38 bytes backscatter packet. The MCU core consumes 23.8%, and 28.3% of the total energy (4.21 μJ) during CRC calculation and data transfer, while the MCU clock accounts for another 22.2%. The LTC6990 oscillator plus the RF switch consume the remaining 25.7%. In our prototype, the MCU consumes three-quarters of the total energy in backscatter mode, highlighting the vast efficiency potentials in designing custom ASICs for backscatter sensor nodes.

Fig. 6.1(c) shows two sample images captured with our battery-free camera.

6.2 Energy Harvesting

We use AM-1801 and AM-1816CA solar panels, designed for indoor operation with areas of 2 in^2 and 17 in^2 respectively, to supply the energy harvester board and evaluate the battery-free sensor nodes update rates. We set up the solar-powered sensors in an office building with fluorescent ceiling lights. The illuminance at the solar cell is 300 lux. We record data for 6 hours using each solar panel and sensor. Table 6.1 lists the achieved average update rates using each solar panel, as well as the idle power consumption, sensing energy, and communication energy for each sensor. The small solar cell supplies enough energy to read the environmental sensors, including temperature, humidity, and illuminance, every second.

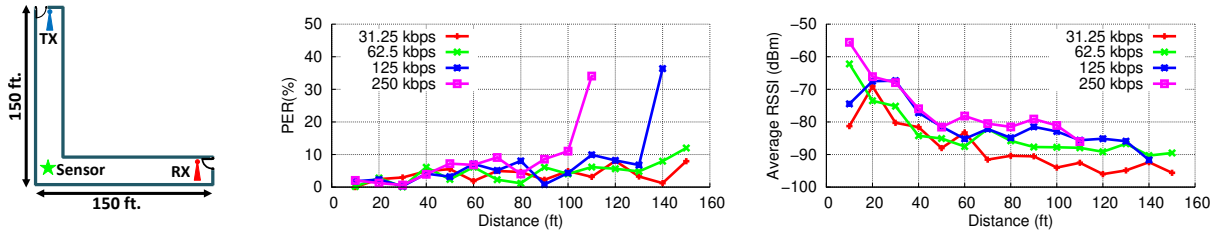

(a) Experiment setup. (b) PER vs Distance. (c) RSSI vs Distance.

Figure 6.2: **Line-of-sight communication range.**

6.3 Range

We set up the system in a 300×5 ft hallway with floor plan shown in Fig. 6.2(a) to evaluate the communication range of the WideScatter system in line-of-sight. The sensor node is in the middle of the hallway (indicated with the green star). In each measurement, we place the RX and TX units at the same distance from the sensor node and measure the Packet Error Rate (PER) of backscatter communication over 1000 packets.

Fig. 6.2(b) shows the PER for four data rates as we increase the RX and TX distances from the sensor node, from 10 ft to 150 ft. Our results show that the WideScatter system can operate up to 150 ft (length of the hallway) at the data rate of 31.25 Kbps (PER ¡ 10%) with an average RSSI of -95 dBm. The maximum achievable range reduces to 100 ft when the sensor node transmits data at 250 Kbps with the average reported RSSI of -80 dBm.

Fig. 6.2(c) shows that the RSSI values at 10 ft for 31.25 Kbps and 62.5 Kbps data rates are less than the next several measuring points, although the distance is increasing. This happens due to the carrier power tuning in the WideScatter system, as explained in sec. 3.1. At this short distance between the devices, the backscatter link achieves low PER with lower carrier power.

Table 6.1: **Power consumption measurements for camera, microphone, and environmental sensors.**

Measurement		Cam.	Mic.	Env.
Idle Power (μ W)		39	51	25
Sensing Energy (mJ)		6.05	3.51	0.025
Communication Energy (mJ)		3.82	2.84	0.014
Solar-Powered Update Rate (sec.)	2 $in^2 panel$	280	268	1
	17 $in^2 panel$	17	11	0.2

6.4 Coverage

To evaluate the performance of WideScatter in a non-line-of-sight scenario, we set up the system in a two-floor educational complex, covering multiple rooms separated by glass and wood doors, as well as concrete walls, with a total area of 23400 ft^2. Fig. 6.3(a) and (b) show the floor plan of the ground and first floor of the building. In our setup, we have 5 RX units (red squares) placed at the height of 3 ft from the floor, and 20 TX units (blue squares) attached to the concrete walls at 6 ft height. This combination of base units costs $569 at low volumes based on our cost analysis (see sec. 5). We place the sensor node at 5 ft height and move it between 130 test points (green circles), while it communicates with the base units at 125 Kbps.

The sensor node transmits 1000 backscatter packets at each test point, and we measure the PER and RSSI of the backscatter packets. Our results show that all test points have PER less than 15 %, and the median of RSSI is -77 dBm (Fig. 6.3(c)), which demonstrates that the WideScatter system is fully capable of covering the entire building.

Also, we evaluate the performance of WideScatter in a 800ft^2 single bedroom apartment (Fig. 6.4(a)) using 1 RX unit and 4 TX units, with an estimated cost of $114. Similar to the other evaluation, the sensor node transmits 1000 packets at 18 test points while maintaining

(a) Ground Floor. (b) First Floor. (c) RSSI.

Figure 6.3: **Backscatter coverage in a two-floor educational complex. RX units, TX units and tested sensor node spots are shown with red squares, blue squares and green circles, respectively.**

(a) Floor plan (b) RSSI.

Figure 6.4: **Single bedroom apartment coverage.**

PER of less than 10 % and median RSSI of -72 dBm as shown in Fig. 6.4(b).

6.5 Throughput

We deploy 5 RX, 20 TX, and 10 sensor node units operating at 125 Kbps in the building shown in Fig. 6.3 to evaluate the performance of WideScatter in a multi-RX multi-TX scenario. The RX and TX units are placed as shown Fig. 6.3(a) and (b), while the sensor node location is shown in the same figures with numbers 1 to 10. In this experiment, we assign two sensor nodes to each RX unit, select a subset of the sensor nodes with 1 to 5 members, command them to transmit data to their assigned RX units, and measure the achieved data rate at each RX unit. To calculate the aggregate throughput, we add up the individual throughput of all RX units involved. Each point in Fig. 6.5 shows the results of

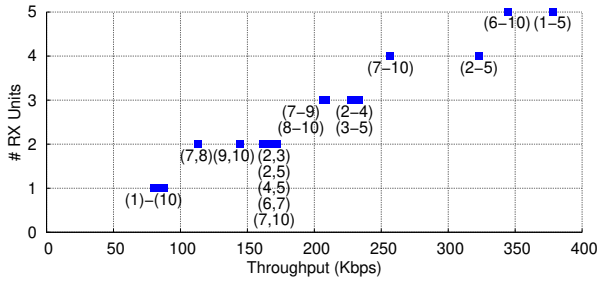

Figure 6.5: **Aggregate throughput with multiple RX.**

one measurement, where the numbers in the parenthesis indicate the location of the sensor nodes involved in the measurement.

Our results in a single RX setup show that the maximum achievable throughput using one sensor node is 90 Kbps. All sensor nodes achieve a throughput close to this nominal data rate when they operate alone. Comparing the nominal data rate to the physical data rate of 125 Kbps shows a 28 % overhead. Our analysis shows that 10 % of this overhead is caused by the TX activation and sensor wake up in the communication cycle. The other 18 % is due to wasted time interval between backscatter packets.

The aggregated throughput of the network also increases linearly as the number of RX units and sensor nodes in the measurement increases. The measurement with sensor nodes placed at locations (1-5) achieves an aggregated throughput of 375 Kbps using 5 RX, which is 4.17 $\times$ faster than a single sensor node. This result shows that multiple backscatter sensor nodes can operate simultaneously and share the spectrum resources among themselves.

In cases where two close sensor nodes communicate with two different RX units, such as (7,8) and (9,10), we observe a lower aggregated throughput compared to the cases where sensor nodes are placed further away from each other, such as (2,3) or (7,10). Our analysis shows that this is mainly due to interference in waking up the sensor nodes since the sensor node wake-up radio uses amplitude modulation.

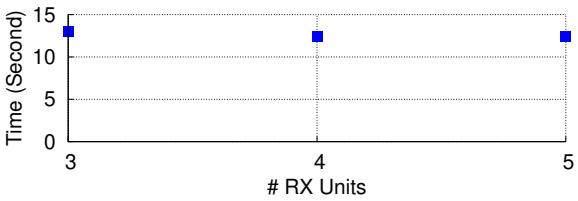

Figure 6.6: **Handover duration.**

6.6 Handover

To demonstrate that WideScatter can manage the movement of sensor nodes between RX units, we set up the system in an office building with three isolated rooms, walk within these rooms at an average pace while carrying the sensor node. We repeat the experiment 10 times for each scenario where the system uses 3, 4, and 5 RX units.

Our results in Fig. 6.6 show that the average time difference between the last successfully received packet at the previous location and the first one at the new location is 13, 12.4, and 12.4 seconds when our setup has 3, 4, and 5 RX units, respectively. This time includes both the relocating time, 8.2 seconds on average, and assigning a new RX unit to the sensor node placed in the new location. This result suggests that the RX assignment process is not significant compared to the movement time in our experiments.

Chapter 7

RELATED WORK

Our work is related to prior efforts in backscatter communication, battery-free sensing, and wireless sensor networks.

Backscatter Communication. Our work builds on recent efforts in advancing bistatic backscatter solutions to deliver ultra-low-power wireless connectivity. These efforts were focused on designing backscatter solutions compatible with existing wireless standards [13, 76, 30, 33, 24, 1, 80, 77, 45, 70, 56, 18], and improving backscatter throughput [47, 23, 82, 84], range [70, 73], reliability [64, 30] and deployability [15, 32]. While these works use a single RX-TX pair in their deployments, we use multiple RX and TX base units to realize wide area and scalable bistatic backscatter systems.

A wireless protocol to handle the concurrent transmission of backscatter devices was presented in [23], which uses chirp spread spectrum modulation to share the channel bandwidth between many devices communicating with a single monostatic backscatter access point. The access point can cover a wide area since each backscatter node has a low data rate that allows the backscattered signals to be recovered at very low signal powers. In this work, we use a network of backscatter base units to extend the coverage at data rates up to 250 Kbps. Although we use 802.15.4g standard with FSK modulation and time-division multiplexing in this work, the techniques presented can be combined with other modulation and multiple access methods.

A scalable backscatter sensor mesh was introduced in [81] that uses distributed excitation to enable multi-hop backscatter between sensor nodes. Although this solution enables the sensor nodes to communicate with each other at longer distances, it requires an excitation source close to each sensor node resulting in significant deployment limitations. In our

architecture, the sensor nodes only communicate with the base units. The network of base units handles the tasks that allow the sensor nodes to move freely inside the coverage area without adding any complexity to the sensor nodes.

Battery-free sensing. Battery-free solutions rely on the harvested energy from RF [67, 53, 71, 65, 52], solar [74, 49, 11], vibration [54, 44], motion [69], thermal [49] and magnetic [20] energy sources for their operation. [79] lists mean energy generated by 50 activities in residential buildings. Applications such as video [65, 22, 26] and audio [71] streaming, gaming [11], full-body temperature mapping [20], food quality monitoring [59], pulse oximetry [36, 75], structural health monitoring [48], flying insects EMG telemetry [72], indoor acoustic localization [83], eye-tracking [43], visible light sensing [74] and many others [69, 46, 40, 19, 42] have been realized with battery-free platforms. In this work, we develop a modular battery-free sensing platform based on bistatic backscatter wireless communication, and use camera, microphone and environmental sensors as example case studies to show the platform capabilities.

Wireless Sensor Networks. Advances in wireless communication, embedded electronics, and physical sensors have fueled the adaptation of wireless sensor networks (WSN) over the past decades [3, 68, 39, 4, 28, 37, 21]. WSN deployments are reported in various applications, including health care monitoring [66, 29, 16], precision agriculture [25, 27, 50], environmental monitoring [34, 60, 2], and industrial monitoring [62, 61]. We design a wireless sensor network based on low-power backscatter technology, which allows us to develop battery-free sensor nodes and further expands the WSN applications.

Chapter 8

CONCLUSION

We present the first wide-area bistatic backscatter system with multiple base unis for battery-free wireless sensor networks. We start from a single RX - single TX backscatter system and expand the network coverage by introducing multiple TX and multiple RX units. We propose techniques to maintain backscatter communication reliability and throughput as the network size grows. We build low-cost hardware using COTS components and prototype proof-of-concept battery-free sensor nodes for capturing images, audio, and environmental parameters.

BIBLIOGRAPHY

[1] Ali Abedi, Mohammad Hossein Mazaheri, Omid Abari, and Tim Brecht. Witag: Rethinking backscatter communication for wifi networks. In *Proceedings of the 17th ACM Workshop on Hot Topics in Networks - HotNets '18*. ACM Press, 2018.

[2] Kofi Sarpong Adu-Manu, Cristiano Tapparello, Wendi Heinzelman, Ferdinand Apietu Katsriku, and Jamal-Deen Abdulai. Water quality monitoring using wireless sensor networks. *ACM Transactions on Sensor Networks*, 13(1):1–41, feb 2017.

[3] I.F. Akyildiz, W. Su, Y. Sankarasubramaniam, and E. Cayirci. Wireless sensor networks: a survey. *Computer Networks*, 38(4):393–422, mar 2002.

[4] Hande Alemdar and Cem Ersoy. Wireless sensor networks for healthcare: A survey. *Computer Networks*, 54(15):2688–2710, oct 2010.

[5] Rabe Arshad, Hesham ElSawy, Sameh Sorour, Tareq Y. Al-Naffouri, and Mohamed-Slim Alouini. Handover management in dense cellular networks: A stochastic geometry approach. In *2016 IEEE International Conference on Communications (ICC)*. IEEE, may 2016.

[6] Ari Asp, Yaroslav Sydorov, Mikko Keskikastari, Mikko Valkama, and Jarno Niemela. Impact of modern construction materials on radio signal propagation: Practical measurements and network planning aspects. In *2014 IEEE 79th Vehicular Technology Conference (VTC Spring)*. IEEE.

[7] Ari Asp, Yaroslav Sydorov, Mikko Valkama, and Jarno Niemela. Radio signal propagation and attenuation measurements for modern residential buildings. In *2012 IEEE Globecom Workshops*. IEEE.

[8] Dinesh Bharadia, Kiran Raj Joshi, Manikanta Kotaru, and Sachin Katti. Backfi: High throughput wifi backscatter. *ACM SIGCOMM Computer Communication Review*, 45(5):283–296, aug 2015.

[9] Alberto Coustasse, M. Tomblin, and Chelsea Slack. Impact of radio-frequency identification (rfid) technologies on the hospital supply chain: A literature review. *Perspectives in health information management / AHIMA, American Health Information Management Association*, 10:1d, 10 2013.

[10] Andrei Croitoru, Dragos Niculescu, and Costin Raiciu. Towards wifi mobility without fast handover. In *12th USENIX Symposium on Networked Systems Design and Implementation (NSDI 15)*, pages 219–234, Oakland, CA, May 2015. USENIX Association.

[11] Jasper de Winkel, Vito Kortbeek, Josiah Hester, and Przemysław Pawełczak. Battery-free game boy. *Proceedings of the ACM on Interactive, Mobile, Wearable and Ubiquitous Technologies*, 4(3):1–34, sep 2020.

[12] Joshua F. Ensworth, Alexander T. Hoang, Thang Q. Phu, and Matthew S. Reynolds. Full-duplex bluetooth low energy (BLE) compatible backscatter communication system for mobile devices. In *2017 IEEE Topical Conference on Wireless Sensors and Sensor Networks (WiSNet)*. IEEE, jan 2017.

[13] Joshua F. Ensworth and Matthew S. Reynolds. BLE-backscatter: Ultralow-power IoT nodes compatible with bluetooth 4.0 low energy (BLE) smartphones and tablets. *IEEE Transactions on Microwave Theory and Techniques*, 65(9):3360–3368, sep 2017.

[14] Akshay Gadre, Revathy Narayanan, Anh Luong, Anthony Rowe, Bob Iannucci, and Swarun Kumar. Frequency configuration for low-power wide-area networks in a heartbeat. In *17th USENIX Symposium on Networked Systems Design and Implementation (NSDI 20)*, pages 339–352, Santa Clara, CA, February 2020. USENIX Association.

[15] Ander Galisteo, Ambuj Varshney, and Domenico Giustiniano. Two to tango: hybrid light and backscatter networks for next billion devices. In *Proceedings of the 18th International Conference on Mobile Systems, Applications, and Services*. ACM, jun 2020.

[16] Gordana Gardašević, Konstantinos Katzis, Dragana Bajić, and Lazar Berbakov. Emerging wireless sensor networks and internet of things technologies—foundations of smart healthcare. *Sensors*, 20(13):3619, jun 2020.

[17] Bradford W. Gildon. InPen smart insulin pen system: Product review and user experience. *Diabetes Spectrum*, 31(4):354–358, sep 2018.

[18] Wei Gong, Longzhi Yuan, Qiwei Wang, and Jia Zhao. Multiprotocol backscatter for personal IoT sensors. In *Proceedings of the 16th International Conference on emerging Networking EXperiments and Technologies*. ACM, nov 2020.

[19] Philipp Gutruf, Rose T. Yin, K. Benjamin Lee, Jokubas Ausra, Jaclyn A. Brennan, Yun Qiao, Zhaoqian Xie, Roberto Peralta, Olivia Talarico, Alejandro Murillo, Sheena W. Chen, John P. Leshock, Chad R. Haney, Emily A. Waters, Changxing Zhang, Haiwen Luan, Yonggang Huang, Gregory Trachiotis, Igor R. Efimov, and John A. Rogers. Wireless, battery-free, fully implantable multimodal and multisite pacemakers for applications in small animal models. *Nature Communications*, 10(1), dec 2019.

[20] Seungyong Han, Jeonghyun Kim, Sang Min Won, Yinji Ma, Daeshik Kang, Zhaoqian Xie, Kyu-Tae Lee, Ha Uk Chung, Anthony Banks, Seunghwan Min, Seung Yun Heo, Charles R. Davies, Jung Woo Lee, Chi-Hwan Lee, Bong Hoon Kim, Kan Li, Yadong Zhou, Chen Wei, Xue Feng, Yonggang Huang, and John A. Rogers. Battery-free, wireless sensors for full-body pressure and temperature mapping. *Science Translational Medicine*, 10(435):eaan4950, apr 2018.

[21] Xin He, Weiwei Jiang, Meng Cheng, Xiaobo Zhou, Panlong Yang, and Brian Kurkoski. Guardrider: reliable wifi backscatter using reed-solomon codes with qos guarantee. In *2020 IEEE/ACM 28th International Symposium on Quality of Service (IWQoS)*, pages 1–10. IEEE, 2020.

[22] Mehrdad Hessar, Saman Naderiparizi, Ye Wang, Ali Saffari, Shyamnath Gollakota, and Joshua R. Smith. Wireless video streaming for ultra-low-power cameras. In *Proceedings of the 16th Annual International Conference on Mobile Systems, Applications, and Services*. ACM, jun 2018.

[23] Mehrdad Hessar, Ali Najafi, and Shyamnath Gollakota. Netscatter: Enabling large-scale backscatter networks. In *Proceedings of the 16th USENIX Conference on Networked Systems Design and Implementation*, NSDI'19, pages 271–283, Berkeley, CA, USA, 2019. USENIX Association.

[24] Vikram Iyer, Vamsi Talla, Bryce Kellogg, Shyamnath Gollakota, and Joshua Smith. Inter-technology backscatter: Towards internet connectivity for implanted devices. In *Proceedings of the 2016 ACM SIGCOMM Conference*, SIGCOMM '16, pages 356–369, New York, NY, USA, 2016. ACM.

[25] Haider Jawad, Rosdiadee Nordin, Sadik Gharghan, Aqeel Jawad, and Mahamod Ismail. Energy-efficient wireless sensor networks for precision agriculture: A review. *Sensors*, 17(8):1781, aug 2017.

[26] Colleen Josephson, Lei Yang, Pengyu Zhang, and Sachin Katti. Wireless computer vision using commodity radios. In *Proceedings of the 18th International Conference on Information Processing in Sensor Networks - IPSN '19*. ACM Press, 2019.

[27] Nattapol Kaewmard and Saiyan Saiyod. Sensor data collection and irrigation control on vegetable crop using smart phone and wireless sensor networks for smart farm. In *2014 IEEE Conference on Wireless Sensors (ICWiSE)*. IEEE, oct 2014.

[28] Zerina Kapetanovic, Ali Saffari, Ranveer Chandra, and Joshua R. Smith. Glaze: Overlaying occupied spectrum with downlink iot transmissions. *Proceedings of the ACM on Interactive, Mobile, Wearable and Ubiquitous Technologies*, 3(4):1–21, dec 2019.

[29] Ramgopal Kashyap. Applications of wireless sensor networks in healthcare. In *Advances in Wireless Technologies and Telecommunication*, pages 8–40. IGI Global, 2020.

[30] Mohamad Katanbaf, Vivek Jain, and Joshua R. Smith. Relacks: Reliable backscatter communication in indoor environments. *Proceedings of the ACM on Interactive, Mobile, Wearable and Ubiquitous Technologies*, 4(2):1–24, jun 2020.

[31] Mohamad Katanbaf, Ali Saffari, and Joshua R. Smith. Receiver selectivity limits on bistatic backscatter range. In *2020 IEEE International Conference on RFID (RFID)*. IEEE, sep 2020.

[32] Mohamad Katanbaf, Anthony Weinand, and Vamsi Talla. Simplifying backscatter deployment: Full-duplex lora backscatter.

[33] Bryce Kellogg, Vamsi Talla, Shyamnath Gollakota, and Joshua R. Smith. Passive wi-fi: Bringing low power to wi-fi transmissions. In *Proceedings of the 13th Usenix Conference on Networked Systems Design and Implementation*, NSDI'16, pages 151–164, Berkeley, CA, USA, 2016. USENIX Association.

[34] Kavi K. Khedo, Rajiv Perseedoss, and Avinash Mungur. A wireless sensor network air pollution monitoring system. *International Journal of Wireless & Mobile Networks*, 2(2):31–45, may 2010.

[35] Daeyoung Kim, M.A. Ingram, and W.W. Smith. Measurements of small-scale fading and path loss for long range RF tags. *IEEE Transactions on Antennas and Propagation*, 51(8):1740–1749, aug 2003.

[36] Jeonghyun Kim, Philipp Gutruf, Antonio M. Chiarelli, Seung Yun Heo, Kyoungyeon Cho, Zhaoqian Xie, Anthony Banks, Seungyoung Han, Kyung-In Jang, Jung Woo Lee, Kyu-Tae Lee, Xue Feng, Yonggang Huang, Monica Fabiani, Gabriele Gratton, Ungyu Paik, and John A. Rogers. Miniaturized battery-free wireless systems for wearable pulse oximetry. *Advanced Functional Materials*, 27(1):1604373, nov 2016.

[37] Taekyung Kim and Wonjun Lee. Anyscatter: Eliminating technology dependency in ambient backscatter systems. In *IEEE INFOCOM 2020-IEEE Conference on Computer Communications*, pages 287–296. IEEE, 2020.

[38] David C. Klonoff and David Kerr. Smart pens will improve insulin therapy. *Journal of Diabetes Science and Technology*, 12(3):551–553, feb 2018.

[39] Mustafa Kocakulak and Ismail Butun. An overview of wireless sensor networks towards internet of things. In *2017 IEEE 7th Annual Computing and Communication Workshop and Conference (CCWC)*. IEEE, jan 2017.

[40] Siddharth R. Krishnan, Chun-Ju Su, Zhaoqian Xie, Manish Patel, Surabhi R. Madhvapathy, Yeshou Xu, Juliet Freudman, Barry Ng, Seung Yun Heo, Heling Wang, Tyler R. Ray, John Leshock, Izabela Stankiewicz, Xue Feng, Yonggang Huang, Philipp Gutruf, and John A. Rogers. Wireless, battery-free epidermal electronics for continuous, quantitative, multimodal thermal characterization of skin. *Small*, 14(47):1803192, oct 2018.

[41] Antonio Lazaro, David Girbau, and David Salinas. Radio link budgets for UHF RFID on multipath environments. *IEEE Transactions on Antennas and Propagation*, 57(4):1241–1251, apr 2009.

[42] Sanghoon Lee, Hao Wang, Jiahui Wang, Qiongfeng Shi, Shih-Cheng Yen, Nitish V. Thakor, and Chengkuo Lee. Battery-free neuromodulator for peripheral nerve direct stimulation. *Nano Energy*, 50:148–158, aug 2018.

[43] Tianxing Li and Xia Zhou. Battery-free eye tracker on glasses. In *Proceedings of the 24th Annual International Conference on Mobile Computing and Networking - MobiCom '18*. ACM Press, 2018.

[44] Xin Li, Li Teng, Hong Tang, Jingying Chen, Haoyu Wang, Yu Liu, Minfan Fu, and Junrui Liang. Vipsn: A vibration-powered iot platform. *IEEE Internet of Things Journal*, 2020.

[45] Yan Li, Zicheng Chi, Xin Liu, and Ting Zhu. Passive-zigbee: Enabling zigbee communication in IoT networks with 1000x+ less power consumption. In *Proceedings of the 16th ACM Conference on Embedded Networked Sensor Systems - SenSys '18*. ACM Press, 2018.

[46] Xiaoyou Lin and Boon-Chong Seet. Battery-free smart sock for abnormal relative plantar pressure monitoring. *IEEE Transactions on Biomedical Circuits and Systems*, 11(2):464–473, apr 2017.

[47] Xin Liu, Zicheng Chi, Wei Wang, Yao Yao, and Ting Zhu. Vmscatter: A versatile {MIMO} backscatter. In *17th {USENIX} Symposium on Networked Systems Design and Implementation ({NSDI} 20)*, pages 895–909, 2020.

[48] Gaël Loubet, Alexandru Takacs, Ethan Gardner, Andrea De Luca, Florin Udrea, and Daniela Dragomirescu. LoRaWAN battery-free wireless sensors network designed for structural health monitoring in the construction domain. *Sensors*, 19(7):1510, mar 2019.

[49] Michele Magno, Xiaying Wang, Manuel Eggimann, Lukas Cavigelli, and Luca Benini. InfiniWolf: Energy efficient smart bracelet for edge computing with dual source energy

harvesting. In *2020 Design, Automation & Test in Europe Conference & Exhibition (DATE)*. IEEE, mar 2020.

[50] Mobasshir Mahbub. A smart farming concept based on smart embedded electronics, internet of things and wireless sensor network. *Internet of Things*, 9:100161, mar 2020.

[51] Joseph Mauro, Kelly B. Mathews, and Eric S. Sredzinski. Effect of a smart pill bottle and pharmacist intervention on medication adherence in patients with multiple myeloma new to lenalidomide therapy. *Journal of Managed Care & Specialty Pharmacy*, 25(11):1244–1254, nov 2019.

[52] Timothy Miller, Stephen S Oyewobi, Adnan M Abu-Mahfouz, and Gerhard P Hancke. Enabling a battery-less sensor node using dedicated radio frequency energy harvesting for complete off-grid applications. *Energies*, 13(20):5402, 2020.

[53] Saman Naderiparizi, Aaron N. Parks, Zerina Kapetanovic, Benjamin Ransford, and Joshua R. Smith. WISPCam: A battery-free RFID camera. In *2015 IEEE International Conference on RFID (RFID)*. IEEE, apr 2015.

[54] Francesco Orfei, Chiara Benedetta Mezzetti, and Francesco Cottone. Vibrations powered LoRa sensor: An electromechanical energy harvester working on a real bridge. In *2016 IEEE SENSORS*. IEEE, oct 2016.

[55] Christoph Paasch, Gregory Detal, Fabien Duchene, Costin Raiciu, and Olivier Bonaventure. Exploring mobile/WiFi handover with multipath TCP. In *Proceedings of the 2012 ACM SIGCOMM workshop on Cellular networks: operations, challenges, and future design - CellNet '12*. ACM Press, 2012.

[56] Yao Peng, Longfei Shangguan, Yue Hu, Yujie Qian, Xianshang Lin, Xiaojiang Chen, Dingyi Fang, and Kyle Jamieson. Plora: a passive long-range data network from ambient lora transmissions. In *Proceedings of the 2018 Conference of the ACM Special Interest Group on Data Communication - SIGCOMM18*. ACM Press, 2018.

[57] G.P. Pollini. Trends in handover design. *IEEE Communications Magazine*, 34(3):82–90, mar 1996.

[58] Poonam, Kriti Sharma, Anmol Arora, and S.K. Tripathi. Review of supercapacitors: Materials and devices. *Journal of Energy Storage*, 21:801–825, feb 2019.

[59] Radislav A. Potyrailo, Nandini Nagraj, Zhexiong Tang, Frank J. Mondello, Cheryl Surman, and William Morris. Battery-free radio frequency identification (RFID) sensors for food quality and safety. *Journal of Agricultural and Food Chemistry*, 60(35):8535–8543, aug 2012.

[60] Maneesha Vinodini Ramesh. Design, development, and deployment of a wireless sensor network for detection of landslides. *Ad Hoc Networks*, 13:2–18, feb 2014.

[61] Daniel Ramotsoela, Adnan Abu-Mahfouz, and Gerhard Hancke. A survey of anomaly detection in industrial wireless sensor networks with critical water system infrastructure as a case study. *Sensors*, 18(8):2491, aug 2018.

[62] Mohsin Raza, Nauman Aslam, Hoa Le-Minh, Sajjad Hussain, Yue Cao, and Noor Muhammad Khan. A critical analysis of research potential, challenges, and future directives in industrial wireless sensor networks. *IEEE Communications Surveys & Tutorials*, 20(1):39–95, 2018.

[63] Ignacio Rodriguez, Huan C. Nguyen, Niels T. K. Jorgensen, Troels B. Sorensen, and Preben Mogensen. Radio propagation into modern buildings: Attenuation measurements in the range from 800 MHz to 18 GHz. In *2014 IEEE 80th Vehicular Technology Conference (VTC2014-Fall)*. IEEE.

[64] Mohammad Rostami, Jeremy Gummeson, Ali Kiaghadi, and Deepak Ganesan. Polymorphic radios: A new design paradigm for ultra-low power communication. In *Proceedings of the 2018 Conference of the ACM Special Interest Group on Data Communication*, SIGCOMM '18, pages 446–460, New York, NY, USA, 2018. ACM.

[65] Ali Saffari, Mehrdad Hessar, Saman Naderiparizi, and Joshua R. Smith. Battery-free wireless video streaming camera system. In *2019 IEEE International Conference on RFID (RFID)*. IEEE, apr 2019.

[66] Nayif Saleh, Abdallah Kassem, and Ali M. Haidar. Energy-efficient architecture for wireless sensor networks in healthcare applications. *IEEE Access*, 6:6478–6486, 2018.

[67] A.P. Sample, D.J. Yeager, P.S. Powledge, A.V. Mamishev, and J.R. Smith. Design of an RFID-based battery-free programmable sensing platform. *IEEE Transactions on Instrumentation and Measurement*, 57(11):2608–2615, nov 2008.

[68] Zhengguo Sheng, Chinmaya Mahapatra, Chunsheng Zhu, and Victor C. M. Leung. Recent advances in industrial wireless sensor networks toward efficient management in IoT. *IEEE Access*, 3:622–637, 2015.

[69] Yu Song, Jihong Min, You Yu, Haobin Wang, Yiran Yang, Haixia Zhang, and Wei Gao. Wireless battery-free wearable sweat sensor powered by human motion. *Science Advances*, 6(40):eaay9842, sep 2020.

[70] Vamsi Talla, Mehrdad Hessar, Bryce Kellogg, Ali Najafi, Joshua R. Smith, and Shyamnath Gollakota. Lora backscatter: Enabling the vision of ubiquitous connectivity. *Proceedings of the ACM on Interactive, Mobile, Wearable and Ubiquitous Technologies*, 1(3):1–24, sep 2017.

[71] Vamsi Talla, Bryce Kellogg, Shyamnath Gollakota, and Joshua R. Smith. Battery-free cellphone. *Proceedings of the ACM on Interactive, Mobile, Wearable and Ubiquitous Technologies*, 1(2):1–20, jun 2017.

[72] S. J. Thomas, R. R. Harrison, A. Leonardo, and M. S. Reynolds. A battery-free multichannel digital neural/EMG telemetry system for flying insects. *IEEE Transactions on Biomedical Circuits and Systems*, 6(5):424–436, oct 2012.

[73] Ambuj Varshney, Carlos Pérez-Penichet, Christian Rohner, and Thiemo Voigt. Lorea: A backscatter architecture that achieves a long communication range. In *Proceedings of the 15th ACM Conference on Embedded Network Sensor Systems - SenSys 17*. ACM Press, 2017.

[74] Ambuj Varshney, Andreas Soleiman, Luca Mottola, and Thiemo Voigt. Battery-free visible light sensing. In *Proceedings of the 4th ACM Workshop on Visible Light Communication Systems*. ACM, oct 2017.

[75] Hao Zhang, Philipp Gutruf, Kathleen Meacham, Michael C. Montana, Xingyue Zhao, Antonio M. Chiarelli, Abraham Vázquez-Guardado, Aaron Norris, Luyao Lu, Qinglei Guo, Chenkai Xu, Yixin Wu, Hangbo Zhao, Xin Ning, Wubin Bai, Irawati Kandela, Chad R. Haney, Debashis Chanda, Robert W. Gereau, and John A. Rogers. Wireless, battery-free optoelectronic systems as subdermal implants for local tissue oximetry. *Science Advances*, 5(3):eaaw0873, mar 2019.

[76] Pengyu Zhang, Colleen Josephson, Dinesh Bharadia, and Sachin Katti. Freerider: Backscatter communication using commodity radios. In *Proceedings of the 13th International Conference on emerging Networking and Technologies - CoNEXT17*. ACM Press, 2017.

[77] Pengyu Zhang, Mohammad Rostami, Pan Hu, and Deepak Ganesan. Enabling practical backscatter communication for on-body sensors. In *Proceedings of the 2016 conference on ACM SIGCOMM 2016 Conference - SIGCOMM '16*. ACM Press, 2016.

[78] Sanliang Zhang and Ning Pan. Supercapacitors performance evaluation. *Advanced Energy Materials*, 5(6):1401401, dec 2014.

[79] Yang Zhang, Yasha Iravantchi, Haojian Jin, Swarun Kumar, and Chris Harrison. Sozu: Self-powered radio tags for building-scale activity sensing. In *Proceedings of the 32nd Annual ACM Symposium on User Interface Software and Technology*. ACM, oct 2019.

[80] Jia Zhao, Wei Gong, and Jiangchuan Liu. Spatial stream backscatter using commodity WiFi. In *Proceedings of the 16th Annual International Conference on Mobile Systems, Applications, and Services - MobiSys 18*. ACM Press, 2018.

[81] Jia Zhao, Wei Gong, and Jiangchuan Liu. Towards scalable backscatter sensor mesh with decodable relay and distributed excitation. In *Proceedings of the 18th International Conference on Mobile Systems, Applications, and Services*. ACM, jun 2020.

[82] Renjie Zhao, Fengyuan Zhu, Yuda Feng, Siyuan Peng, Xiaohua Tian, Hui Yu, and Xinbing Wang. OFDMA-enabled wi-fi backscatter. In *The 25th Annual International Conference on Mobile Computing and Networking - MobiCom19*. ACM Press, 2019.

[83] Yi Zhao and Joshua R. Smith. A battery-free RFID-based indoor acoustic localization platform. In *2013 IEEE International Conference on RFID (RFID)*. IEEE, apr 2013.

[84] Fengyuan Zhu, Yuda Feng, Qianru Li, Xiaohua Tian, and Xinbing Wang. DigiScatter: efficiently prototyping large-scale ofdma backscatter networks. In *Proceedings of the 18th International Conference on Mobile Systems, Applications, and Services*. ACM, jun 2020.